DOI: 10.61782/fa.2025.0504

FORUM ACUSTICUM
EURONOISE 2025

INVESTIGATION OF STOP BAND BEHAVIOR IN COMPLEX FINITE VIBROACOUSTIC METAMATERIAL STRUCTURES USING A POWER-BASED METHOD

Heiko Atzrodt[1*] **Arun Maniam**[1] **Nikolai Kleinfeller**[1] **Sebastian Rieß**[1]

[1] Fraunhofer Institute for Structural Durability and System Reliability LBF, 64289 Darmstadt, Germany

ABSTRACT

Structural intensity (STI) is a powerful tool for identifying energy sources and sinks for studying the transmission paths of vibrational energy within structures. Vibroacoustic metamaterials (VAMMs), which utilize local resonance effects to create stop bands, inhibit free wave propagation within specific frequency ranges. This study introduces an approach that uses active structural intensity to quantitatively assess the stop band behavior in complex, finite VAMM plate-like structures. The proposed vibrational power-based method offers a robust framework for evaluating stop band characteristics by analyzing active power flow and quantifying the energy loss due to the VAMM's resonators. Furthermore, damping plays a crucial role in the application of the STI method, and it is necessary to distinguish between the influences of damping and metamaterials. The effectiveness of this approach is confirmed by comparing the predicted stop band with the frequency response function (FRF) of the structure, demonstrating its accuracy in capturing stop band behavior. The effect of uncertainty in the resonator parameters on the stop band width is explored to assess the sensitivity of the vibrational power-based method in predicting stop band behavior under varying parameters.

Keywords: *active structural intensity, acoustic, complex finite metamaterials, power loss, stop band*

**Corresponding author*: *heiko.atzrodt@lbf.fraunhofer.de.*

1. INTRODUCTION

Vibroacoustic metamaterials (VAMMs) have garnered significant interest in recent years due to their ability to control the propagation of mechanical vibrations through engineered structures [1–3]. By leveraging local resonance effects, VAMMs can create stop bands, effectively blocking elastic waves of certain frequency ranges from propagating through the material [4–6]. Traditional methods such as Bloch-wave, Floquet models, and transfer matrix techniques primarily rely on unit cell (UC) models, assuming infinite periodic structures and neglecting real boundary conditions [7–9]. However, these idealizations often fail to capture the complexities introduced by real-world design variations, non-uniform material properties, and geometric irregularities within finite VAMM structures [10, 11].

Structural intensity (STI) emerges as a powerful tool in this context, offering insights into the distribution of vibrational energy within complex structures. Unlike traditional methods, active STI can be used for the quantification of energy or power within a region with resonators, thereby facilitating a detailed understanding of power loss due to the effectiveness of the resonators [12, 13].

This paper extends the methodology introduced in [12, 13] to apply the power-based approach for predicting stop band behavior in complex finite VAMM structures. Unlike traditional UC models, which often fail to accurately capture the actual responses of these structures, this method provides a reliable framework to precisely assess stop band characteristics. Additionally, the approach illustrates how damping in resonators influences power loss and, consequently, affects stop band predictions.

2. OBJECTIVE

The mechanical structure under investigation is a generic car undercarriage [14] depicted in Fig. 1. Detailed geometrical dimensions can be found in [14]. The chassis represents a simplified yet typical car structure commonly analyzed and optimized for vibroacoustic performance. Hence, exploring how applying VAMM to this car undercarriage mitigates vibrations and quantifying the resulting stop band using a power-based approach are crucial objectives. Tab. 1 presents the material properties of the generic car undercarriage. The goal is to integrate metamaterials onto the car undercarriage by placing resonators in the central section (between boundary regions 1 and 2 as shown in Fig. 2)

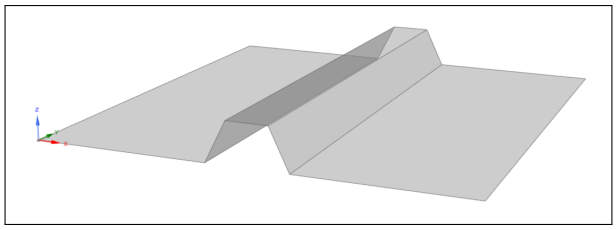

Figure 1. Generic car undercarriage structure.

Table 1. Material properties of the generic car undercarriage.

Property	Value
Young's modulus E	70×10^9 N/m^2
Poisson's ratio μ	0.33
Mass density ρ	2700 kg/m^3
Material loss factor η	0.005

3. METHODOLOGY

STI quantifies both the magnitude and direction of energy flow within a structure when excited by external forces. It comprises two components: active STI ($\vec{I}_{\mathrm{S,a}}$) and reactive STI ($\vec{I}_{\mathrm{S,r}}$). The active component describes the propagation of structure-borne energy, resembling a moving wave on a time-average basis, while the reactive component represents energy oscillations within the structure, similar to a standing wave. Vibrations often originate from thin shell-like structures, such as those commonly found in undercarriages. Eqn. (1) allows for the calculation of power within enclosed areas in shell models [12].

$$\oint_C \vec{I}_{\mathrm{S'},\mathrm{a}}\, \vec{n}\, dl = P_{\mathrm{in}} - P_{\mathrm{diss}} \tag{1}$$

where the apostrophe symbol denotes the active STI in thin structures, C represents the contour of the shell element, $\vec{n}$ describes the vector normal to the closed area, l signifies the length of each element along the contour line, P_{in} stands for the input power (energy inflow into the closed area) and P_{diss} represents the dissipated power (energy outflow from the closed area).

In the context of VAMM systems, the power dynamics are assessed through $P_{\mathrm{in,VAMM}}$ and $P_{\mathrm{out,VAMM}}$, calculated using Eqn. (1). $P_{\mathrm{in,VAMM}}$ represents the power entering the resonator region across boundary region 1 (see Fig. 2), while $P_{\mathrm{out,VAMM}}$ denotes the power exiting through boundary region 2. The difference between these values, $P_{\mathrm{in,VAMM}} - P_{\mathrm{out,VAMM}}$, quantifies the power loss within the VAMM system, referred to as $P_{\mathrm{loss,VAMM}}$. To express this loss as a percentage, $P_{\mathrm{in,VAMM}}$ and $P_{\mathrm{out,VAMM}}$ are normalized relative to $P_{\mathrm{in,VAMM}}$, the total power entering the resonator zone.

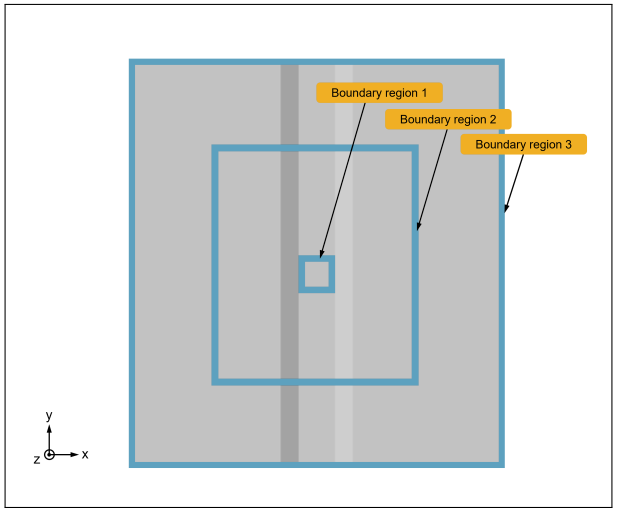

Figure 2. Definition of boundary regions for resonator placement and power flow calculation in the undercarriage with VAMM.

To assess the power loss in the undercarriage with VAMM compared to the host structure, the power loss calculation is replicated for the host structure using a similar

approach. Subsequently, the energy flows in the undercarriage with VAMM are normalized relative to those in the host structure, denoted as $P_{\text{in,Host}}$ and $P_{\text{out,Host}}$, respectively. This normalization provides insight into the relative power loss attributable to the resonators. In essence, the power loss ratio in the resonators, $P_{\text{loss,Res}}$, is expressed as shown in Eqn. (2). After normalization, the value of one in this equation indicates that the energy flowing into the resonator region equals 100%.

$$P_{\text{loss,Res}} = 1 - \frac{P_{\text{out,VAMM}}/P_{\text{in,VAMM}}}{P_{\text{out,Host}}/P_{\text{in,Host}}} \qquad (2)$$

4. UNDERCARRIAGE WITH VAMM

Fig. 3 depicts the undercarriage with VAMM, featuring a 10x10 resonator configuration, designed to attenuate free wave propagation within a frequency range around 100 Hz. All the outer edges of the structure are fixed. A 10 N harmonic nodal force is applied to the middle node present in the boundary region 1 at the location [0.675m, 0.7m, 0.13m].

The resulting undercarriage with VAMM exhibits an additional mass that is 10% of the host structure. Tab. 2 summarizes the properties of the resonators. Three different values for Lehr's damping such as 0.01, 0.03 and 0.05 are chosen to investigate the damping effects on the stop band determination.

Table 2. Properties of the resonators.

Property	Value
Mass m	0.03 kg
Spring stiffness c	11843.53 N/m

5. RESULTS

A quantitative analysis of the vibration attenuation capabilities in a VAMM structure necessitates defining a stop band as a percentage of vibration attenuation. This step is essential for accurately evaluating the structure's vibroacoustic performance, where the percentage value indicates the extent of vibration attenuation achieved. For example, a relative power loss of 99% signifies that the resonators within VAMM structures have blocked 99% of the vibration compared to the host structure. Fig. 4 depicts the power loss ratio in the resonators, $P_{\text{loss,Res}}$, alongside

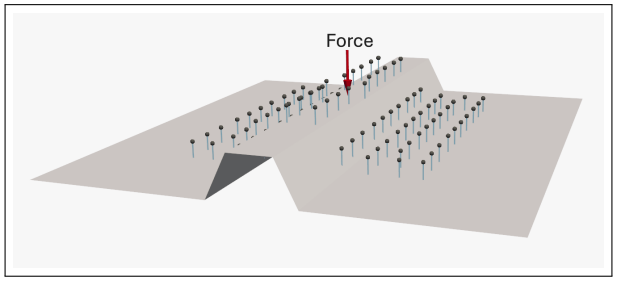

Figure 3. The car undercarriage illustrating mounted resonators alongside the position of the harmonic force.

shaded areas representing their stop bands, determined by a 99% power loss threshold and varying Lehr's damping ratios. The stop band widths, along with their corresponding upper and lower limits for damping ratios of 1%, 3%, and 5%, are summarized in Tab. 3.

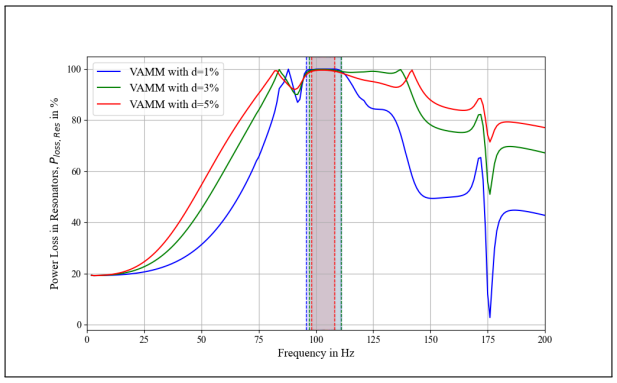

Figure 4. Relative power loss in resonators with different Lehr's damping ratios. Highlighted regions indicate corresponding stop bands.

Fig. 5 compares the frequency response function (FRF) curves of the host structure and the undercarriage with VAMM across three different damping configurations. The FRF is evaluated at nodes located between boundary regions 2 and 3. The stop band, predicted using the power loss method, is highlighted in Fig. 5, showing excellent agreement with frequency regions characterized by a large amplitude reduction in the FRF curve. This illustrates the efficacy of the power loss method in identifying stop bands, even in complex structures like a car undercarriage. As the damping ratio increases, resonators become less effective at achieving 99% vibration attenua-

Table 3. Stop band widths for different damping ratios with upper and lower limits.

Damping Ratio (%)	Lower Limit (Hz)	Upper Limit (Hz)	Stop Band Width (Hz)
1%	95.8	111.0	15.2
3%	97.0	111.0	14.0
5%	98.0	108.0	10.0

tion, resulting in narrower stop bands.

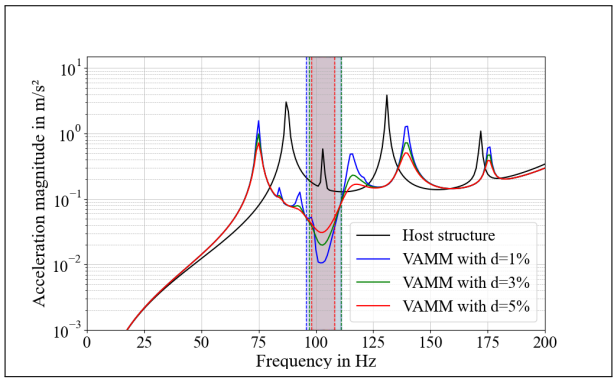

Figure 5. FRF comparison between host structure and undercarriage with VAMM with varying Lehr's damping ratios, highlighting predicted stop bands using a 99% power loss threshold.

In real-world systems, VAMM parameters often vary due to manufacturing inaccuracies. To investigate the robustness of the suggested method in predicting stop bands, the impact of mass variations in the resonators using an uncertainty coefficient of 0.1 is evaluated. The resonator properties, as listed in Tab. 2, include a Lehr's damping ratio of 1%. Ten simulations were conducted, each determining stop bands using a 99% power loss threshold approach. Fig. 6 illustrates the stop band widths from these simulations, contrasting them with the stop band width of the reference undercarriage with VAMM without uncertainty (denoted by the dashed black line).

6. CONCLUSION

In summary, this study has demonstrated the effectiveness of a power-based approach utilizing active structural intensity to quantitatively assess stop band behavior

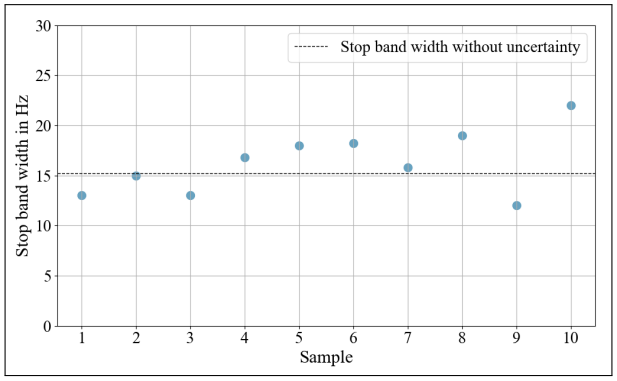

Figure 6. Comparison of stop band widths for samples with a normalized standard deviation of 0.1 of the resonators masses and the reference undercarriage with VAMM without uncertainty

in complex, finite VAMM plate-like structures. Through the analysis of vibrational energy flow and the quantification of energy attenuation attributed to VAMM resonators, a robust framework has been established for evaluating stop band characteristics. The $P_{\text{loss,Res}}$ effectively distinguishes the relative power loss solely due to metamaterials in comparision to the bare car undercarriage. Validation against FRF data confirms the method's accuracy in predicting stop band behavior. This offers valuable insights for optimizing vibroacoustic performance in applications involving real-world VAMM structures, where parameters often vary due to manufacturing inaccuracies. To assess the robustness of the proposed method, the impact of mass variations in the resonators was evaluated using an uncertainty coefficient of 0.1. These findings underscore the method's potential in predicting and optimizing stop bands, even in VAMM structures subject to such uncertainties.

7. REFERENCES

[1] S. Riess, M. Droste, D. Manushyna, S. Melzer, T. Druwe, T. Georgi, and H. Atzrodt, "Vibroacoustic metamaterials for enhanced acoustic behavior of vehicle doors," in *2021 Fifteenth International Congress on Artificial Materials for Novel Wave Phenomena (Metamaterials)*, pp. 374–376, IEEE, 2021.

[2] D. Manushyna, M. Hülsebrock, A. Kuisl, A. D. Vivo, P. Heloret, H. Atzrodt, and S. Rapp, "Application of vibroacoustic metamaterials for structural vibration

reduction in space structures," *Mechanics Research Communications*, vol. 129, p. 104090, 2023.

[3] S. Rieß, R. Schmidt, W. Kaal, H. Atzrodt, and S. Herold, "Vibration reduction on circular disks with vibroacoustic metamaterials," *Applied Sciences*, vol. 14, no. 11, p. 4637, 2024.

[4] C. C. Claeys, K. Vergote, P. Sas, and W. Desmet, "On the potential of tuned resonators to obtain low-frequency vibrational stop bands in periodic panels," *Journal of Sound and Vibration*, vol. 332, no. 6, pp. 1418–1436, 2013.

[5] L. n· Brillouin, *Wave Propagation in Periodic Structures: Electric Filters and Crystal Lattices*. Dover, 1953.

[6] C. Claeys, "Design and analysis of resonant metamaterials for acoustic insulation," *KU Leuven: Leuven, Belgium*, 2014.

[7] M. I. Hussein, M. J. Leamy, and M. Ruzzene, "Dynamics of phononic materials and structures: Historical origins, recent progress, and future outlook," *Applied Mechanics Reviews*, vol. 66, no. 4, p. 040802, 2014.

[8] F. Bloch, "Über die quantenmechanik der elektronen in kristallgittern," *Zeitschrift für physik*, vol. 52, no. 7, pp. 555–600, 1929.

[9] G. Floquet, "Sur les équations différentielles linéaires à coefficients périodiques," in *Annales scientifiques de l'École normale supérieure*, vol. 12, pp. 47–88, 1883.

[10] P. F. Pai, H. Peng, and S. Jiang, "Acoustic metamaterial beams based on multi-frequency vibration absorbers," *International Journal of Mechanical Sciences*, vol. 79, pp. 195–205, 2014.

[11] H. B. Al Ba'ba'a and M. Nouh, "Mechanics of longitudinal and flexural locally resonant elastic metamaterials using a structural power flow approach," *International Journal of Mechanical Sciences*, vol. 122, pp. 341–354, 2017.

[12] H. Atzrodt, A. Maniam, M. Droste, S. Rieß, and M. Hülsebrock, "A power-based framework for quantifying parameter uncertainties in finite vibroacoustic metamaterial plates," *Materials*, vol. 16, no. 14, p. 5139, 2023.

[13] H. Atzrodt, A. Maniam, M. Droste, and S. Rieß, "A power-based approach based on active structural intensity: Stop band prediction of vibroacoustic metamaterial plate," in *2023 Seventeenth International Congress on Artificial Materials for Novel Wave Phenomena (Metamaterials)*, pp. X–022, IEEE, 2023.

[14] C. Adams, J. Bös, and T. Melz, "A benchmark case for structural intensity calculations," in *DAGA*, vol. 43, pp. 375–378, 2017.